

Polarisation of cells and soft objects driven by mechanical interactions: Consequences for migration and chemotaxis

M. Leoni & P. Sens

Laboratoire Gulliver, UMR 7083 CNRS-ESPCI, 10 rue Vauquelin, 75231 Paris Cedex 05 - France

(Dated: January 27, 2022)

We study a generic model for the polarisation and motility of self-propelled soft objects, biological cells or biomimetic systems, interacting with a viscous substrate. The active forces generated by the cell on the substrate are modelled by means of oscillating force multipoles at the cell-substrate interface. Symmetry breaking and cell polarisation for a range of cell sizes naturally “emerge” from long range mechanical interactions between oscillating units, mediated both by the intracellular medium and the substrate. However, the harnessing of cell polarisation for motility requires substrate-mediated interactions. Motility can be optimised by adapting the oscillation frequency to the relaxation time of the system or when the substrate and cell viscosities match. Cellular noise can destroy mechanical coordination between force-generating elements within the cell, resulting in sudden changes of polarisation. The persistence of the cell’s motion is found to depend on the cell size and the substrate viscosity. Within such a model, chemotactic guidance of cell motion is obtained by directionally modulating the persistence of motion, rather than by modulating the instantaneous cell velocity, in a way that resembles the run and tumble chemotaxis of bacteria.

I. INTRODUCTION

Cell motility on solid substrates (crawling) and in fluid environments (swimming) are usually regarded as being based on different physical principles and studied independently. Swimming often relies on the beating or rotation of protrusive appendages (flagella or cilia) [1, 2], while crawling generally relies on the protrusive and contractile forces generated by the acto-myosin cytoskeleton, and on cell-substrate adhesion [1]. Remarkably, several cell types that undergo major shape changes while crawling, such as amoebae and neutrophils, are also able to swim in Newtonian fluids [3, 4]. Furthermore, crawling cells are sensitive to the stiffness (elastic response) [5–7], but also to the viscosity [8, 9] of the substrate on which they are crawling. This suggests that crawling and swimming share common underlying physical principles and that insight on eukaryotic cell motility may be gained by studying self-propelling soft objects in fluid environments [10].

Cell motility requires polarisation, namely the breaking of front-back symmetry of the cell. This can be triggered by external gradients of either biochemical (chemotaxis) [11] or mechanical (*e.g.* durotaxis) [12] nature, or it can occur spontaneously. Spontaneous cell polarisation is of particular interest to understand the spatio-temporal correlations inside and outside the cell. Active gel theories [13–18] have shed some light on the physics of spontaneous cell polarisation, but much remains to be learnt about how coordination is achieved at the scale of the whole cell, and how coordinated motions are affected by the properties of the extra-cellular environment.

Here, we devise a generic theoretical framework which enables us to address in a unified manner three different fundamental aspects: polarisation, motility and chemotaxis. Our model soft cell (henceforth simply ‘cell’), which aims at describing active droplets [15–17, 19], biomimetic self-propelled systems and cells, is a viscous or

an elastic body interacting with a substrate by means of localised forces distributed over the cell-substrate contact area. We restrict ourselves to the case where the substrate is a Newtonian fluid, so that force transmission between the cell and the substrate can be achieved by enforcing a no-slip boundary condition. Our findings also provide insight into the polarisation of cells adhering to elastic substrates, although crawling in that case requires additional assumptions concerning the dynamic of creation and destruction of adhesion sites.

The cell cytoskeleton commonly displays quasi-periodic spatio-temporal patterns and fluctuations of activity [20–22]. These oscillations are observed in both adherent [23–25] and crawling cells [26–28] even in the absence of specific adhesion receptors [29]. Motivated by that, we model the distribution of cellular forces as oscillating force-multipoles at the cell-substrate interface. Spatio-temporal correlations among the oscillating forces may spontaneously emerge from mechanical interactions, affecting cell polarisation and cell motility. To show this, we first study the motility of a cell exerting forces on the substrate with prescribed time-dependence. The resulting cell speed has non-monotonic trend as function of the substrate viscosity or of the frequency of the oscillating units. We then study spontaneous symmetry breaking associated to cell polarisation and the transition from non-motile to motile states as a dynamical process emerging from the phase-locking of the oscillating elements. This process occurs only for a range of cell sizes and is permitted by long-range interactions mediated by both the substrate and the cytoplasm. To investigate chemotaxis, we introduce a minimal coupling between chemotactic gradients and the force distribution. Finally, we discuss the persistence of cell motion in the presence of noise (*e.g.* cellular noise) and we obtain testable predictions regarding the substrate-dependent statistical properties of the cell trajectories.

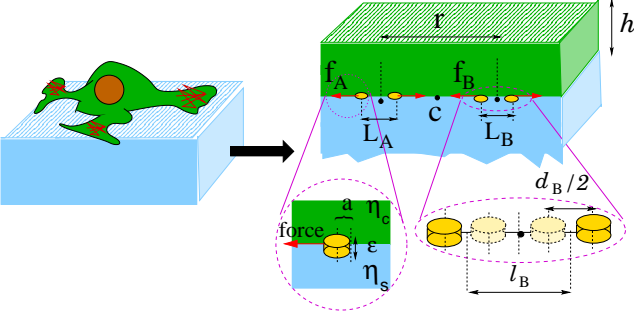


FIG. 1. (Color online) A motile cell exerting traction forces on a flat viscous substrate is modelled as two coupled fluids: a layer of thickness h and viscosity η_c (the “cell” on top, in green) lying over an infinite bulk fluid substrate of viscosity η_s (at the bottom, in light blue). Cytoskeletal elements generating traction are modelled as oscillating force multipoles (two dipoles in the sketch) distributed along a line.

II. MODEL

To begin with, we model the cell as an incompressible fluid layer of thickness h and viscosity η_c lying over an incompressible bulk fluid of viscosity η_s (Fig.1) at low Reynolds number. The fluids are immiscible and satisfy the Stokes equation [30]:

$$\begin{aligned} \eta_c \nabla^2 \mathbf{v}^{(c)} - \nabla p^{(c)} &= 0; \nabla \cdot \mathbf{v}^{(c)} = 0, (0 \leq z \leq h) \\ \eta_s \nabla^2 \mathbf{v}^{(s)} - \nabla p^{(s)} &= 0; \nabla \cdot \mathbf{v}^{(s)} = 0, (-\infty < z < 0) \end{aligned} \quad (1)$$

where $\mathbf{v}^{(c)}, p^{(c)}$ and $\mathbf{v}^{(s)}, p^{(s)}$ are the velocity and pressure fields in the fluid layer and the substrate, and z the direction normal to the interface. The fields $\mathbf{v}^{(c)}$ and $\mathbf{v}^{(s)}$ are coupled by means of conditions at the interface $z = 0$. In the following, we assume no-slip boundary conditions at the interface, $\mathbf{v}^{(c)}|_{z=0} = \mathbf{v}^{(s)}|_{z=0}$, and neglect normal displacements of the interface, $v_z^{(c)}|_{z=0} = v_z^{(s)}|_{z=0} = 0$. Similar results are obtained if no-slip is enforced only at the location of the active force generators, see Appendix A 2.

Protein complexes responsible for the traction forces at the cell-substrate interface are modelled as N disks of finite radius a and negligible height $\epsilon \rightarrow 0$ distributed at positions \mathbf{r}_n ($n = 1, \dots, N$) at the interface between the two fluids via $\mathbf{F}(\mathbf{r}, z = 0) = \sum_{n=1}^N \mathbf{F}_n \delta(\mathbf{r} - \mathbf{r}_n)$. By virtue of Newton’s third law, the cell exerts no net force on the substrate, $\sum_{n=1}^N \mathbf{F}_n = 0$, and the local stress balance at the interface reads

$$\eta_c \frac{d}{dz} \mathbf{v}_{\parallel}^{(c)} - \eta_s \frac{d}{dz} \mathbf{v}_{\parallel}^{(s)} = -\mathbf{F}(\mathbf{r}, z = 0) \quad (2)$$

where $\mathbf{v}_{\parallel}^{(\zeta)}$ denotes the in-plane component of the velocity $\mathbf{v}^{(\zeta)}$ for $\zeta = s, c$, see Appendix A 1. The solution of Eqs.(1,2) can be obtained using Fourier transforms, see e.g. [31, 32], as explained in Appendix A 1. We focus here on the analytically tractable limit of two coupled

semi-infinite fluids, $h \rightarrow \infty$. The interfacial velocity field at a distance r from a unique interfacial point-force \mathbf{f} is $\mathbf{v}(r) = \frac{1}{2\pi(\eta_s + \eta_c)} \frac{1}{r} \mathbf{f}$. The effect of several point-forces is additive thanks to the linearity of Eq.(1).

To study the emergence of cell polarisation we consider time-dependent and periodic force distributions consisting of two identical units A and B , labelled with index α in the following, that on average over a period are mirror symmetric with respect to the cell centre (Fig.1). For simplicity, all forces are distributed along a line. Each unit is made of particles with coordinates $\mathbf{x}_n^\alpha = x_n^\alpha \hat{\mathbf{x}}$, subjected to forces $\mathbf{F}_n^\alpha = F_n^\alpha \hat{\mathbf{x}}$ directed along the $\hat{\mathbf{x}}$ axis. Each unit centre is at $\mathbf{c}_\alpha = 2/N \sum_n \mathbf{x}_n^\alpha$, the cell centre at $\mathbf{c} = (\mathbf{c}_A + \mathbf{c}_B)/2$, and the separation between units is $\mathbf{r} := \mathbf{c}_B - \mathbf{c}_A$.

III. SUBSTRATE VISCOSITY AFFECTS THE CELL SPEED

A. Derivation of the cell speed

Interactions between the point forces may lead to the motion of the force distribution with respect to both the cytoplasm and the substrate. Only the interactions mediated by the substrate can lead to displacement of the whole cell. Since the cell’s radial boundary is not introduced explicitly in our model, the cell net velocity is obtained by subtracting the cytosol motion to the motion of the force centre \mathbf{c} . This leads to a force balance $\zeta \dot{\mathbf{c}} = \sum_\alpha \sum_n \mathcal{S}_n^\alpha$ as explained in detail in Appendix B 1. Here, $\mathcal{S}_n^\alpha = \zeta_s \mathbf{v}(\mathbf{x}_n^\alpha)$ represents the substrate-mediated traction force, and $\mathbf{v}(\mathbf{x}_n^\alpha) := \mathbf{v}^{(c)}(\mathbf{x}_n^\alpha) = \mathbf{v}^{(s)}(\mathbf{x}_n^\alpha)$ is the velocity at the location of disk (α, n) due to the motion of all remaining disks. The total and substrate-related drag coefficients are ζ and ζ_s . In the limit $h \rightarrow \infty$ for a disk of radius a : $\zeta_s = \frac{16}{3} \eta_s a$ and $\zeta = \frac{16}{3} (\eta_s + \eta_c) a$ [33].

We first consider the case where each unit is an oscillating force dipole made of two particles: $n = 1, 2$ with one force scale $F_1^\alpha = -F_2^\alpha := f_\alpha$ and one length scale $L_\alpha = x_1^\alpha - x_2^\alpha$. With no loss of generality we write $L_\alpha = l_\alpha + d_\alpha$ where l_α is a constant and d_α describes time-dependent deformations, see Fig.1. We parametrize the amplitude and force of the oscillating dipoles as:

$$d_\alpha = R_\alpha \cos(\omega t + \phi_\alpha); \quad f_\alpha = -g_\alpha \sin(\omega t + \phi_\alpha). \quad (3)$$

The average cell velocity is obtained from the net displacement of the cell centre over an oscillation period. For the pair of identical dipoles ($\{g, R, l\}_A = \{g, l, R\}_B$) shown in Fig.1, for $h \rightarrow \infty$ and to lowest order in l_α/r , it has a simple expression derived in Appendix B 4:

$$v_c(\psi) := \frac{1}{T} \int_0^T dt \dot{c}(t) \sim \frac{\eta_s}{(\eta_s + \eta_c)^2} \frac{g R l^2}{r^4} \Xi \sin \psi \quad (4)$$

where $\psi := \phi_B - \phi_A$ is the phase difference between the oscillators. Geometrical details of the force distribution are contained in $\Xi = \frac{3}{32\pi} [4 + (R/l)^2 \cos \psi]$, see Appendix

B 4d. Replacing the viscous cell with an elastic cell of elastic modulus μ_c yields a similar result, with $\mu_c/(i\omega)$ in place of η_c , see Appendix A 3, Appendix B 2, Appendix B 4e.

The relationship between forces and displacements is obtained from the force-balance equation: $\zeta \dot{\mathbf{d}}_\alpha = 2\mathbf{f}_\alpha + \mathcal{I}_\alpha$. Here $\mathcal{I}_\alpha = \zeta[\mathbf{v}(\mathbf{x}_1^\alpha) - \mathbf{v}(\mathbf{x}_2^\alpha)]$ represent non-local interactions, propagated both by intracellular and extracellular media. For small amplitude oscillations: $R_\alpha \ll l_\alpha < r$, interactions may be neglected to lowest order and the force-amplitude relation is $g_\alpha = (\zeta\omega R_\alpha)/2$.

The active forces (typically actin polymerisation and actomyosin contraction for crawling cells) may impose either the force or the displacement scale. Eq.(4) shows that the migration speed is qualitatively different for imposed displacement ($v_c \sim \eta_s/(\eta_s + \eta_c) \times a\omega(Rl)^2/r^4$) and imposed force ($v_c \sim \eta_s/(\eta_s + \eta_c)^3 \times (gl)^2/(a\omega r^4)$). In the latter case, the velocity presents a maximum when the substrate and cell viscosity are similar (see Fig.2(a) - the value of the optimal ratio depends on ψ). This biphasic behaviour shows an interesting analogy with the biphasic velocity of cells crawling on elastic substrates in response to substrate stiffness [5–7]. The speed of an elastic cell can be optimised by tuning the frequency of the oscillating force units close to the inverse relaxation time of the system: $\omega \sim 2\frac{\mu_c}{\eta_s}$, see Fig.2(b). This suggests that cells may adjust their oscillations rate to the mechanical properties of the environment for optimal motility. By symmetry, a fluid cell with oscillating disks permanently bound to an elastic substrate experiences a net cytoplasmic flow. However, harnessing this flow for cell migration on an elastic substrate requires additional hypothesis concerning disk attachment to and detachment from the substrate, or disk creation at the cell front and destruction at the rear.

Using typical values of parameters obtained from experiments we estimate $v_c \sim 10(\mu\text{m})/\text{hr}$. This is smaller than typical cellular speed, a common drawback for swimmers, made up of point-like particles, undergoing small amplitude strokes [34]. Higher speeds can be obtained by increasing a/r and l_α/r beyond the validity of the analytical results, Eq.(4). This expression is however very valuable, as it shows that net migration requires that the oscillators *phase lock* at $\psi \neq 0(\pi)$, like interacting dumb-bells in bulk fluids [35, 36]. This breaks time-reversal symmetry, a requirement for motility at low Reynolds number (“scallop theorem” [37]).

B. Estimated value for the average migration speed

Probing the cell with periodic stress or strain of well defined frequency ω allows one to infer the viscosity of the cytosol η_c , from measured values of the shear loss modulus G_c'' by means of the relation $\eta_c \sim G_c''/\omega$.

To estimate values of migration speed in our model, we consider oscillation frequencies $\nu_0 \sim 1\text{Hz}$, (a lower bound for swimming cells [2]) i.e. $\omega = 2\pi(\text{rad})/\text{s}$. Intra-

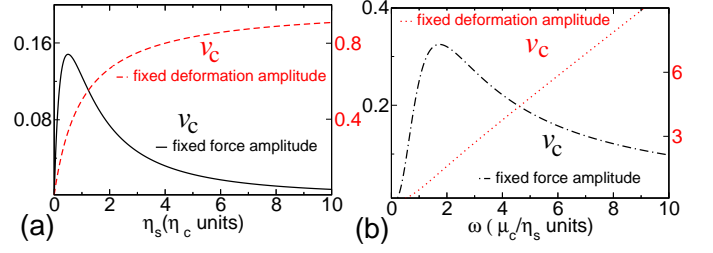


FIG. 2. (Color online) (a) Average migration speed (Eq.(4)) as function of the substrate viscosity η_s . The force distribution is shown in Fig.1, with $\psi = \pi/2$, for either fixed force (continuous black line) or fixed displacement (dashed red line). The former is measured in units of $(9g^2l^2)/(64\pi\eta_c^2\omega ar^4)$ and the latter in units of $(a\omega l^2R^2)/(\pi r^4)$. η_s is measured in units of η_c . (b) Average migration speed variation with the driving frequency for an elastic cell of elastic modulus μ_c . Velocities for fixed force (dashed dotted black line) and fixed displacement (dotted red line) are measured respectively in units of $(9g^2l^2)/(64\pi\eta_s\mu_c ar^4)$ and in units of $(a\mu_c R^2l^2)/(\eta_s\pi r^4)$ while ω is measured in units of μ_c/η_s , the viscoelastic frequency.

cellular measurements give $G_c'' \sim 100\text{Pa}$ at $\nu_0 \sim 1\text{Hz}$, see [38]. The associated cell viscosity is $G_c''/\omega = \frac{100}{2\pi}\text{Pa s}$ (a highly viscous regime: for comparison water at room temperature has a viscosity $\sim 10^{-3}\text{Pa s}$ – four orders of magnitude below). For simplicity we take a substrate with equivalent viscosity, i.e. we consider conditions of ‘viscosity matching’ between the cell and the substrate.

We next address the relation among force and deformation for the oscillator. We consider forces $g \sim 0.5nN$ that are varying with frequency $\omega \sim 2\pi(\text{rad})/\text{s}$ dragging a disk of size $0.5\mu\text{m}$. The drag coefficient is $\zeta = [16a(\eta_s + \eta_c)]/3 \sim (10aG_c'')/\omega$. The corresponding oscillation amplitude is $R = \frac{2g}{\omega\zeta} \sim \frac{10^{-9}\text{N}}{10 \times 0.5\mu\text{m} \times 100\text{Pa}} \sim 2\mu\text{m}$.

The average migration speed can be calculated using the formula valid for fixed deformation amplitudes, reported above. In addition to the previous values, we consider $l \sim 2R \sim 4\mu\text{m}$ and $r \sim 10\mu\text{m}$ (as well as ‘viscosity matching’ $\eta_s = \eta_c$) from which $v_c \sim \frac{a}{\pi} \frac{R^2l^2\omega}{r^4} \frac{\eta_s}{(\eta_s + \eta_c)} \sim (10\mu\text{m})/\text{hr}$. Under same conditions of lengths, and matching between cell-substrate moduli $\eta_s \sim \frac{\mu_c}{\omega}$, the elastic cell has the same speed of the viscous cell $v_c \sim \frac{a}{\pi} \frac{R^2l^2\omega^3}{r^4} \frac{\eta_s^2}{(\omega^2\eta_s^2 + \mu_c^2)} \sim (10\mu\text{m})/\text{hr}$.

IV. CELL POLARISATION, MOTILITY AND CHEMOTAXIS EMERGE FROM SYNCHRONISATION

We now show that polarisation and migration of the cell may spontaneously emerge as the result of dynamical interactions and synchronisation of the force generators. The amplitudes $R_\alpha(t)$ and $g_\alpha(t)$, and the phase $\phi_\alpha(t)$ are now slowly varying quantities : constant over an oscillation period $T = 2\pi/\omega$, but varying over longer time scales as a result of intracellular interactions [39, 40]. A

simple model [40] leading to self-sustained oscillations is the evolution equation for the forces,

$$\dot{f}_\alpha = \frac{1}{2}[-\mathcal{K}_\alpha d_\alpha + \mathcal{M}f_\alpha[1 - \sigma d_\alpha^2] + \mathcal{A}d_\alpha^3] \quad (5)$$

combined with the force balance equation $\zeta \dot{\mathbf{d}}_\alpha = 2\mathbf{f}_\alpha + \mathcal{I}_\alpha$ (for $\alpha = A, B$). These equations are equivalent to a van der Pol-Duffing oscillator [40, 41] that exhibits supercritical Hopf's bifurcation [41] in a wide range of the parameter space. Similar models emerge from the collective dynamics of molecular motors, see e.g. [42, 43]. Here, \mathcal{K}_α sets the oscillation frequency, \mathcal{M} determines the instability threshold and σ is a stabilising term. These parameters must be strictly positive for a stable limit cycle to exist. $\mathcal{A} \neq 0$ describes non-isochronous oscillations [40], and determines whether the oscillation frequency increases ($\mathcal{A} < 0$) or decreases ($\mathcal{A} > 0$) with increasing amplitude R_α . This non-linear coupling may for instance result from the mechano-sensitive kinetics of sub-cellular constituents.

In the absence of chemotactic bias, the parameters \mathcal{K} , σ and \mathcal{A} are identical at both ends A and B of the cell. We implement chemotaxis by writing $\mathcal{K}_\alpha = \mathcal{K} + \tilde{\mathcal{K}}\rho_\alpha$ where $\rho_\alpha = \rho(c_\alpha)$ is the density of chemoattractant at the centre c_α of unit α . This description is consistent with recent studies on chemotaxis [44], where pseudopods at the cell edges display wave-like patterns and chemoattractant changes the rate of internal processes (here the oscillation rate, see below).

The dynamics of a single oscillator is seen neglecting interactions \mathcal{I}_α . Combining Eqs.(3,5) with $\zeta \dot{d}_\alpha = 2f_\alpha$, and averaging over the (fast) period T yields $\dot{R}_\alpha = \mathcal{M}R_\alpha[1 - \sigma(R_\alpha)^2/4]$, showing that the amplitude saturates at a stable value $\mathfrak{R} = 2(\sqrt{\sigma})^{-1}$, and the phase rotates at slow frequency $\dot{\phi}_\alpha = -\mathcal{K}_\alpha + \mathcal{A}\mathfrak{R}^2$. To study synchronisation of distant oscillators, we assume that the interactions \mathcal{I}_α induce small deviations from the limit cycle [40], see [45] for details, yielding a phase equation:

$$\dot{\psi} = \Omega + \text{sgn}[\mathcal{A}]\frac{1}{\tau_0}(U + \cos \psi) \sin \psi. \quad (6)$$

Here $\Omega = \frac{\tilde{\mathcal{K}}}{2\omega\zeta}(\rho^A - \rho^B)$ is the chemotactic bias, the relaxation time τ_0 results from the long-range interactions between oscillators, and U contains geometrical details of the force distribution. Eq.(6) resembles Adler's equation [39], previously used to describe synchronisation [40, 46] and swimming of algae having intrinsic front-back asymmetry [47, 48] in low Reynolds number fluids. The additional term $\sin \psi \cos \psi$ is associated to force multipoles. For two dipolar units (Fig.1); $\tau_0 = (\pi\mathcal{M}\zeta r^3)/(2|\mathcal{A}|\mathfrak{R}^4 a)$ and $U = 2l^2/\mathfrak{R}^2$.

It is instructive to write Eq.(6) as $\dot{\psi} = -\frac{1}{\tau_0}\frac{d}{d\psi}V(\psi)$, in terms of an effective potential V with minima corresponding to (meta)stable phase-locking between the two oscillating units (Fig.3). Motility requires $\psi \neq 0(\pi)$, see Eq.(4). In the absence of chemotactic bias ($\Omega = 0$), V

presents a single minimum (modulo 2π) if $|U| > 1$ (continuous blue curve in Fig.3b). A bistable systems with $\psi \neq 0(\pi)$ spontaneously emerges from the long-range interactions if $\mathcal{A} > 0$ and $|U| < 1$, with two symmetric stable states corresponding to spontaneous cell polarisation and motion (dashed-dotted green curve in Fig.3b), separated by an effective energy barrier $\Delta V_0 = (1 - |U|)^2/2$. Moderate gradients of chemoattractants ($0 < \tau_0|\Omega| < 1$) introduce a bias that displaces the single minimum ($|U| > 1$) or favours one of the two stable states ($|U| < 1$), (continuous blue and dashed-dotted green curves in Fig.3d), thus directing motility.

The pair of dipolar oscillators considered so far (Fig.1) has $U > 1$ and does not exhibit a stable state with broken symmetry. Spontaneous cell polarisation is possible if the force distribution in each unit is itself polarised, the whole cell conserving mirror symmetry. In Fig.3a, we show an example where each unit consists of two dipoles (I and II), separated by a distance ξ . To keep the number of parameters minimal, dipole I is chosen to be a scaled version of dipole II : $l_I/l_{II} = \mathfrak{R}_I/\mathfrak{R}_{II} = \kappa$ with $l_{II} = l$; $\mathfrak{R}_{II} = \mathfrak{R}$. The two dipoles oscillate at the same frequency ω and with a fixed phase difference; oscillator I is in opposition of phase with oscillator II , which satisfies Eq.(5). This way, the two units are characterised by a single dynamical phase difference ψ satisfying Eq.(6). As shown in [45], the migration speed for this force distribution is still given by Eq.(4) with $\Xi = \frac{3}{32\pi}\{4(\kappa^2 - 1)^2 + \frac{\mathfrak{R}^2}{l^2}[\kappa^2 + 1]^2 \cos \psi\}$ and retains the qualitative trend shown in Fig.2. More interestingly, phase locking at $\psi \neq 0(\pi)$ occurs when $|U| = |\frac{2l^2}{\mathfrak{R}^2} \frac{1 - (1 - \delta)^3 \kappa^2}{1 + (1 - \delta)^3 \kappa^2}| < 1$ (where $\delta := \xi/r$) and $\mathcal{A} > 0$. Correspondingly, $\frac{1}{\tau_0} = \frac{|\mathcal{A}|}{\mathcal{M}} \frac{2a\mathfrak{R}^4}{\pi\zeta} \frac{1 + (1 - \delta)^3 \kappa^2}{r^3(1 - \delta)^3}$.

V. NOISY OSCILLATIONS RESULT IN DIRECTED OR PERSISTENT MOTIONS

Uncorrelated noise, associated e.g. to the stochastic nature of actin polymerisation and motor proteins activity, influences intracellular synchronisation. Adding a random effective "force", ν , to Eq.(6): $\dot{\psi} = \frac{1}{\tau_0}[-\frac{d}{d\psi}V(\psi) + \nu]$, results in fluctuations around a stable minimum and occasional jumps between two minima of V leading to phase slips [39, 46]. When $|U| > 1$, jumps give a phase slip of 2π and do not change the cell velocity. Velocity fluctuations are controlled by local fluctuation of ψ around the minimum ψ^* , estimated to be of order $\langle(\psi - \psi^*)^2\rangle \simeq \Lambda/\partial_\psi^2 V(\psi^*) \sim \Lambda/||U| - 1|$, where Λ is the intensity of the noise, with correlation $\langle\nu(t)\nu(t')\rangle = 2\Lambda\tau_0\delta(t - t')$. The cell performs a random walk along the \hat{x} axis in the absence of chemotactic gradients, or a random walk with drift with such gradients, with a diffusion coefficient of order $D \simeq \langle v_c^2 \rangle \tau_0 \sim (\partial_\psi v_c(\psi^*))^2 \tau_0 \Lambda / (|U| - 1)$ (continuous blues curves in Fig.3c,e). When $|U| < 1$, the two stable states ψ_\pm (with $\sin \psi_- = -\sin \psi_+$) have non-vanishing velocities

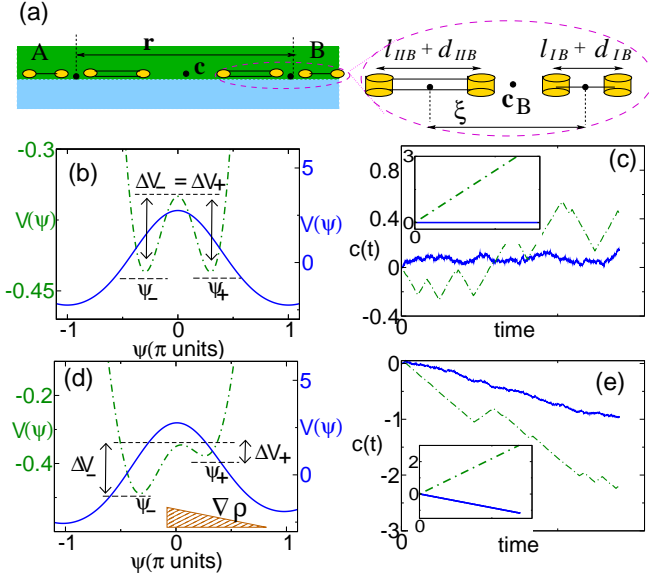


FIG. 3. (Color online) (a) Force-distribution corresponding to two polarised oscillators at either edge of the cell, a system that can show spontaneous symmetry breaking ($|U| < 1$). (b-e) Synchronisation landscape and cell trajectories obtained from numerical simulations (see [45] for details). All panels have $\mathcal{A} > 0$ and either $U > 1$ (continuous blue curves) or $|U| < 1$ (dashed-dotted green curves). (b) Effective cell polarisation landscape $V(\psi)$, and (c) trajectories of the cell centre $c(t)$ with time in the absence of chemotactic gradient ($\Omega = 0$). In the presence of chemotactic gradient, (d), the effective landscape $V(\psi)$ is asymmetric and (e) the cell trajectories show a bias. Insets in (c,e) are trajectories in the absence of noise. In this case, the direction of motion for $|U| < 1$ is arbitrary, and may be away from the chemotactic gradient. All parameters are the same for the continuous blue curves and dashed-dotted green curves except r (double for the dashed dotted green curves) resulting in $U = -0.6$ (dashed-dotted green curves) and $U = 2.5$ (continuous blue curves).

$v_c(\psi_-) = -v_c(\psi_+)$ (Eq.(4)). The cell's trajectory is thus a succession of persistent motions separated by random changes of direction, resembling the run and tumble motion of bacteria [49]. The persistence time of directed motion is the first passage time between two consecutive jumps: $\mathcal{T}_{\pm} \propto \tau_0 e^{\Delta V_{\pm}/\Lambda}$ [50]. Typical trajectories without and with chemotactic gradients, obtained from numerical simulations (see [45] for details), are shown in Fig.3c,e (dashed-dotted green curves).

VI. DISCUSSION

Our model captures within a single framework two distinct chemotactic strategies, namely the case where the gradient polarises an otherwise quiescent cell ($|U| > 1$) and the case where the gradient biases a preexisting polarised state showing transient directed motion ($|U| < 1$). Interestingly, in the latter case the directional bias intro-

duced by chemotactic gradients is mostly due to a bias in the “run” time \mathcal{T}_{\pm} , due to the asymmetry of the potential barrier ($\Delta V_- > \Delta V_+$ in Fig.3e), and only slightly to directional bias in the cell velocities ($|v_c(\psi_-)| > |v_c(\psi_+)|$). This chemotactic strategy, reminiscent of the one of bacteria [49], has to some extent been observed for *Dic-tyostelium* [44, 51].

The value of $|U|$ is critical to spontaneous cell polarisation, the persistence of cell motion, and the cell chemotactic response. Factors that affect the value of U will thus qualitatively affect the cell's trajectories. For a given force distribution in each unit at the cell edges, increasing the cell size r monotonously decreases U . The condition $|U| < 1$ corresponds to a range of cell size, and we thus predict that very small or very large cells (compared to the size of one force unit) should not show spontaneous polarisation. Another remarkable result is that in the fixed force regime (when $\Re \propto 1/\zeta$), the parameter $U \sim \zeta^2$ increases with increasing substrate viscosity. We further predict that not only is the instantaneous cell velocity affected by the substrate mechanics as depicted in Fig.2, but also the *persistence* of cell motion, and the ability for spontaneous cell polarisation in the absence of external cues, could be strongly impaired under high substrate mechanical resistance.

ACKNOWLEDGMENTS

The work was supported by the Human Frontier Science Program under the grant RGP0058/2011. We thank B. Ladoux, M. Sixt and T.B. Liverpool (M.L.) for stimulating discussions.

Appendix A: Flow at the cell-substrate interface

1. Two coupled fluid layers

In this Appendix we outline the procedure to obtain the analytical solution of Eq.(1) considered in the main text. Related problems were studied previously also by other authors, see e.g. ref [31, 32].

We consider two planar fluid interfaces, at position $z = 0$ and at position $z = \mathfrak{h}$ where \hat{z} is a unit vector indicating the direction normal to the interface. To proceed it is useful to decompose the velocity appearing in Eq.(1) $\mathbf{v}^{\varsigma}(x, y, z) = \mathbf{v}_{\parallel}^{\varsigma}(x, y, z) + v_z^{\varsigma}(x, y, z)\hat{z}$ in terms of the in-plane components $\mathbf{v}_{\parallel}^{\varsigma}(x, y, z)$ and orthogonal component $v_z^{\varsigma}(x, y, z)$ where the label $\varsigma = c, s$ indicates either cell or the substrate. A similar decomposition can be done for the gradient: $\nabla = \nabla_{\parallel} + \hat{z} \frac{\partial}{\partial z}$ where $\nabla_{\parallel} = (\frac{\partial}{\partial x}; \frac{\partial}{\partial y})$ has components only in the (x, y) plane. Finally the Laplacian becomes $\nabla^2 = \nabla_{\parallel}^2 + \frac{\partial^2}{\partial z^2}$.

The boundary conditions at the interfaces are as follows: no motions along z-axis, $\mathbf{v}^{(c)} \cdot \hat{z}|_{z=\mathfrak{h}} = 0$, and continuity of the tangential component of the velocity

at the interface; no-stress condition at the cell-upper solvent interface (obtained neglecting solvent viscosity) $\eta_c[\nabla_{\parallel} v_z^{(c)} + \frac{d}{dz} v_{\parallel}^{(c)}]_{z=h} = 0$. At the cell-substrate interface, $z = 0$, the conditions are no z -motions of the interface, $\mathbf{v}^{(c)} \cdot \hat{\mathbf{z}}|_{z=0} = 0$ and $\mathbf{v}^{(s)} \cdot \hat{\mathbf{z}}|_{z=0} = 0$; continuity of the tangential component, $\mathbf{v}_{\parallel}^{(c)}|_{z=0} = \mathbf{v}_{\parallel}^{(s)}|_{z=0}$; stress balance, $\eta_c[\nabla_{\parallel} v_z^{(c)} + \frac{d}{dz} v_{\parallel}^{(c)}]_{z=0} - \eta_s[\nabla_{\parallel} v_z^{(s)} + \frac{d}{dz} v_{\parallel}^{(s)}]_{z=0} = -\mathbf{F}(\mathbf{r}, z = 0)$. As explained in the main text, it suffices to focus on a single interfacial point force $\mathbf{F}(\mathbf{r}, z = 0) = \mathbf{f}\delta(\mathbf{r})$.

We search a solution using Fourier transforms. By exploiting the geometry of the system, we decompose the Fourier vector \mathbf{k} as $\mathbf{k} = \mathbf{q} + p\hat{\mathbf{z}}$ where \mathbf{q} lies in the plane (x, y) orthogonal to direction $\hat{\mathbf{z}}$. Thanks to this decomposition, a generic vector field $\mathbf{E}(x, y, z)$ in three-dimensions in presence of the planar interface at $z = 0$ can be written as

$$\mathbf{E}(x, y, z) = \int \frac{d^3\mathbf{k}}{(2\pi)^3} e^{-i\mathbf{k}\cdot\mathbf{x}} \tilde{\mathbf{E}}(\mathbf{k}) = \int \frac{d^2\mathbf{q}}{(2\pi)^2} e^{-i\mathbf{q}\cdot\mathbf{r}} \tilde{\mathbf{E}}(\mathbf{q}, z). \quad (\text{A1})$$

We proceed by taking the Fourier transform of the velocity components. The condition of no motion in the z -direction at the interfaces means $\tilde{v}_z^{(c)}(\mathbf{q}, 0) = 0$ and $\tilde{v}_z^{(s)}(\mathbf{q}, h) = 0$ so the various stress conditions only involve terms $\tilde{\mathbf{v}}_{\parallel}^{(s)}(\mathbf{q}, z)$ for $\varsigma = c, s$.

We now make an ansatz concerning the z -dependence of the Fourier components. For the flow in the substrate $z \leq 0$ we pose $\tilde{\mathbf{v}}_{\parallel}^{(s)}(\mathbf{q}, z) := \mathbf{S}(\mathbf{q})e^{qz}$. For the intracellular flow, in the region $0 < z < h$, we pose $\tilde{\mathbf{v}}_{\parallel}^{(c)}(\mathbf{q}, z) = \mathbf{C}_+(\mathbf{q})e^{-qz} + \mathbf{C}_-(\mathbf{q})e^{qz}$. The three terms $\mathbf{C}_{\pm}, \mathbf{S}$ can be determined using the boundary conditions for the stress and velocity given before.

As we have three unknowns, it suffices to consider three of the four equations for the tangential velocities discussed above. We choose the continuity of the tangential velocity at $z = 0$, $\mathbf{C}_+ + \mathbf{C}_- = \mathbf{S}$ and the two equations for the interfacial stresses at $z = h$: $0 = \eta_c[-\mathbf{C}_+e^{-qh} + \mathbf{C}_-e^{qh}]$; at $z = 0$: $q\eta_c[-\mathbf{C}_+ + \mathbf{C}_-] - q\eta_s\mathbf{S} = -\mathbf{f}$. From the second equation we obtain $\mathbf{C}_+ = e^{2qh}\mathbf{C}_-$. Using this relation in the first equation we get $\mathbf{S} = \mathbf{C}_-(1 + e^{2qh})$. Inserting these relations in the third equation, we determine $\mathbf{C}_-, \mathbf{C}_+$ and finally the flow at the cell-substrate interface $z = 0$

$$\tilde{\mathbf{v}}_{\parallel}^{(s)}(\mathbf{q}, 0) \equiv \mathbf{S} \equiv \mathbf{C}_+ + \mathbf{C}_- = \frac{\mathbf{f}}{q\{\eta_c[\tanh(hq)] + \eta_s\}}.$$

The inverse Fourier transform of $\mathbf{S}(\mathbf{q})$ has two analytically tractable limits: $h \rightarrow 0$, corresponding to a thin film, and $h \rightarrow \infty$, representing two semi-infinite coupled fluids. We focus on the latter where $[\tanh(hq)] = 1$ and

$$\begin{aligned} \mathbf{v}_{\parallel}^{(c)}(\mathbf{r}, 0) &\equiv \mathbf{v}_{\parallel}^{(s)}(\mathbf{r}, 0) = \frac{\mathbf{f}}{(2\pi)^2(\eta_s + \eta_c)} \int d^2\mathbf{q} \frac{1}{q} e^{-i\mathbf{q}\cdot\mathbf{r}} \\ &= \frac{\mathbf{f}}{2\pi(\eta_s + \eta_c)} \int_0^\infty dq J_0(qr) = \frac{\mathbf{f}}{2\pi(\eta_s + \eta_c)r} \end{aligned} \quad (\text{A2})$$

Here we used $\int d^2\mathbf{q} \frac{1}{q} e^{-i\mathbf{q}\cdot\mathbf{r}} = \int_0^\infty dq q \int_0^{2\pi} d\theta \frac{1}{q} e^{-iqr \cos \theta} = 2\pi \int_0^\infty dq J_0(qr)$ where J_0 indicates the modified Bessel function of the first kind of zeroth order [52]. Eq.(A2) is the expression reported in the main text and represents the disturbance in the flow field at the interface of two semi-infinite fluids, generated at position \mathbf{r} by a point force placed at the origin, and $r := \|\mathbf{r}\|$. We can write this relation as $\mathbf{v}(\mathbf{r}) = H(\mathbf{r})\mathbf{f}$ where $H(\mathbf{r})$ is the Greens's function describing the flow at the interface. Thanks to the linearity of the equations describing the fluids, the effect of N point forces is obtained by superposing the single effects. The velocity disturbance generated at the interface at position \mathbf{x} due to N disks, each one centred at position \mathbf{x}_n and subjected to forces \mathbf{f}_n with $n = 1, \dots, N$, is given by $\mathbf{v}(\mathbf{x}) = \sum_{n=1}^N \frac{1}{2\pi(\eta_c + \eta_s)\|\mathbf{x} - \mathbf{x}_n\|} \mathbf{f}_n$.

2. Narrow gap between two fluid layers

In this section we study the case where the cell interacts with the substrate only through discrete sites (disks) corresponding to the force-generating elements while the remaining part of the interface is allowed to slip ($\mathbf{v}^{(c)} \neq \mathbf{v}^{(s)}$) without friction. To this end we consider a narrow gap, a quasi-2D film of height h and small viscosity η_a , separating the two fluids (see Fig.4). For simplicity we shall treat the film as a 2D fluid [31, 53, 54]. The coupled Stokes equations now read

$$\begin{aligned} \eta_c \nabla^2 \mathbf{v}^{(c)} - \nabla p^{(c)} &= 0; \quad \text{with } \nabla \cdot \mathbf{v}^{(c)} = 0; \quad z > 0 \\ \eta_a \nabla_{\parallel}^2 \mathbf{v}^{(a)} - \nabla_{\parallel} p^{(a)} + \eta_c \partial_z \mathbf{v}^{(c)} - \eta_s \partial_z \mathbf{v}^{(s)} &= -\mathbf{f}\delta(\mathbf{x}); \\ \text{with } \nabla_{\parallel} \cdot \mathbf{v}^{(a)} &= 0; \quad z = 0 \\ \eta_s \nabla^2 \mathbf{v}^{(s)} - \nabla p^{(s)} &= 0; \quad \text{with } \nabla \cdot \mathbf{v}^{(s)} = 0; \quad z < 0 \end{aligned} \quad (\text{A3})$$

where $\mathbf{v}^{(c)}, p^{(c)}$ indicate velocity and pressure for the intracellular flow; and $\mathbf{v}^{(s)}, p^{(s)}$ velocity and pressure for the substrate flow as before. $\mathbf{v}^{(a)}, p^{(a)}$ are the 2D velocity and pressure in the film, so η_a is a two-dimensional viscosity and the ratio $\eta_a/(\eta_c + \eta_s)$ has the dimension of a length [31, 53–55]. The terms $\eta_c \partial_z \mathbf{v}^{(c)}$ and $-\eta_s \partial_z \mathbf{v}^{(s)}$ describe the stress exerted by the cell and the substrate on the film. Equal and opposite stresses are exerted by the film on the upper and lower bulk fluids, which enter as boundary conditions for the first and the last line of Eq.(A3).

We impose the continuity of the velocities at the location of the disks, $\mathbf{v}^{(c)}|_{\text{disk}} = \mathbf{v}^{(s)}|_{\text{disk}} = \mathbf{v}^{(a)}|_{\text{disk}}$. This way, using the ansatz $\tilde{\mathbf{v}}^{(s)}(\mathbf{q}) = \mathbf{S}(\mathbf{q})e^{zq}$; $\tilde{\mathbf{v}}^{(c)}(\mathbf{q}) = \mathbf{C}(\mathbf{q})e^{-zq}$; $\tilde{\mathbf{v}}^{(a)}(\mathbf{q}) = \mathbf{A}(\mathbf{q})$ we get the equation in Fourier space for the film. Taking the inverse Fourier transform, $\mathbf{v}^{(a)}(\mathbf{r}) = \int \frac{d^2\mathbf{q}}{(2\pi)^2} e^{-i\mathbf{q}\cdot\mathbf{r}} \frac{[\mathbb{I} - \hat{\mathbf{q}}\hat{\mathbf{q}}]}{[q^2\eta_a + q(\eta_c + \eta_s)]} \cdot \mathbf{f}$. The integral can be calculated analytically, the result is expressed in terms of special functions. The limit of negligible film viscosity can be obtained directly by setting $\eta_a = 0$ in the above expression. The flow $\mathbf{v}^{(a)} = v^{(a)}\hat{\mathbf{x}}$ resulting from a force in the same direction $\mathbf{f} = f\hat{\mathbf{x}}$ is again of the

form $v^{(a)}(r) \sim \frac{1}{(\eta_s + \eta_c)r} f$.

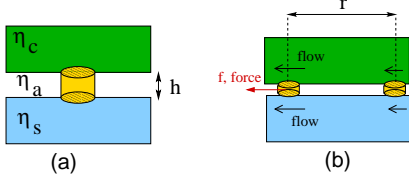


FIG. 4. (Color online) (a) scheme of a viscous cell of viscosity η_c , lying on a viscous substrate of viscosity η_s separated by a small gap h of viscosity η_a . The disks represent force-generating elements which are in contact with both the cell and the substrate. (b) When subjected to a force, each disk drags its surrounding molecules and generates a local flow. This flow propagates and affects also other disks far apart.

3. Equations describing elastic cells lying on viscous substrates

Here we generalise our description to the case of an elastic cell characterised by bulk elasticity μ_c . The disks are arranged with the same geometry considered in Fig.1, they oscillate around their equilibrium positions of Fig.1 but are now permanently bound to the cell elastic body. The dynamics at the interface ($z = 0$) is derived as in Section A 1. In absence of motions along z -axis, the force balance is described by $\mu_c \partial_z \mathbf{u}_{\parallel}^{(c)} - \eta_s \partial_z \mathbf{v}_{\parallel}^{(s)} = -\mathbf{F}(\mathbf{r}, z, t)$ where $\mathbf{u}^{(c)}$ represents the deformation field in the elastic medium. The decomposition of $\mathbf{u}^{(c)}$ into components that are parallel, $\mathbf{u}_{\parallel}^{(c)}$, and orthogonal, $u_z^{(c)}$, to the interface is defined as in Section A 1. The velocities in the upper medium (cell) and in the lower medium (substrate) coincide at the locations of the disks

$$\partial_t \mathbf{u}_{\parallel}^{(c)}|_{\text{disk}} = \mathbf{v}_{\parallel}^{(s)}|_{\text{disk}}. \quad (\text{A4})$$

Once the force-distribution is known, these equations determine both deformation in the cell and the flow generated in the substrate at the location of the disks.

Once again to proceed we define Fourier transforms, now with respect to both space and time, $g(\mathbf{x}, t) = \int \frac{d^2 \mathbf{q} d\Omega}{(2\pi)^4} e^{-i\mathbf{q} \cdot \mathbf{r}} e^{-i\Omega t} \tilde{g}(\mathbf{q}, \Omega)$ for any function g . From Eq.(A4), $-i\Omega \tilde{\mathbf{u}}_{\parallel}^{(c)} = \tilde{\mathbf{v}}_{\parallel}^{(s)}$. To obtain the z -dependence of the solutions we proceed as in Section A 1, posing $\tilde{\mathbf{v}}_{\parallel}^{(s)}(\mathbf{q}, z, \Omega) = \mathbf{S}(\mathbf{q}, \Omega) e^{qz}$ and $\tilde{\mathbf{u}}_{\parallel}^{(c)}(\mathbf{q}, z, \Omega) = \mathbf{C}(\mathbf{q}, \Omega) e^{-qz}$. Therefore at the disk locations $-i\Omega \mathbf{C}(\mathbf{q}, \Omega) = \mathbf{S}(\mathbf{q}, \Omega)$, resulting in $\mathbf{S}(\mathbf{q}, \Omega) = \tilde{\mathbf{F}}(\mathbf{q}, \Omega) / [q(\eta_s + i\frac{\mu_c}{\omega})]$.

As we are interested in the oscillatory behaviour of the cell, we consider a point-like force which oscillates with frequency ω , $\mathbf{F}(\mathbf{x}, t) = \mathbf{f}_0 \delta(\mathbf{x}) \sin(\omega t)$. As a result $\tilde{\mathbf{F}}(\mathbf{q}, \Omega) = \mathbf{f}_0 \frac{2\pi}{2i} [\delta(\Omega + \omega) - \delta(\Omega - \omega)]$. Using this we can take the inverse transform and obtain the velocity field

at the interface at the position of a disk as (for simplicity we remove superscripts)

$$\mathbf{v}_{\parallel}(\mathbf{x}, t) = \int \frac{d^2 \mathbf{q} d\Omega}{(2\pi)^2} \frac{e^{-i\mathbf{q} \cdot \mathbf{r}} e^{-i\Omega t}}{q[\eta_s + i\frac{\mu_c}{\omega}]} \frac{\mathbf{f}_0}{2i} [\delta(\Omega + \omega) - \delta(\Omega - \omega)].$$

Performing the integrals, we can recast the resulting expression using Green's function as

$$\mathbf{v}(\mathbf{x}, t) = \mathbf{H}^{(e)}(r) \cdot \mathbf{F} + \partial_t [\mathbf{G}^{(e)}(r) \cdot \mathbf{F}]; \quad (\text{A5})$$

$$H_{ij}^{(e)}(r) = \frac{\eta_s}{\eta_s^2 + \frac{\mu_c^2}{\omega^2}} \frac{1}{2\pi r} \delta_{ij}; \quad G_{ij}^{(e)}(r) = \frac{\frac{\mu_c}{\omega}}{\eta_s^2 + \frac{\mu_c^2}{\omega^2}} \frac{1}{2\pi r} \delta_{ij}$$

where δ_{ij} is the Kronecker symbol. We note that letting $\mu_c \rightarrow 0$ one recovers the expression for the semi-infinite viscous substrate, and similarly letting $\eta_s \rightarrow 0$ one obtains the equivalent expression for the elastic medium.

Appendix B: Dynamics of the four disks system

We focus on the system made up of two oscillating units, labeled with $\alpha = A, B$, each unit consisting of a single dipole discussed in the text, see Fig.1. Although in the main text we restricted to a one-dimensional force distribution, in the following section we derive the equations in vectorial form valid for generic force distributions.

1. Derivation of the equations describing the crawler's dynamics

The dynamics at the interface of two fluids with negligible inertia and viscosities η_c and η_s is instructive to highlight similarities and differences between the locomotion of a soft object and the swimming in bulk viscous fluids at low Reynolds number [37].

We begin with noting that the motion of a disk lying at the interface of the two fluids can be very complicated : a disk straddling the interface can cause deformations or instabilities of the interface which in turn affect the disk motion. A simple approximation consists in *neglecting* this aspect of the interface dynamics. Such an approximation is valid if the surface tension is constant and sufficiently large to prevent any interface deformation. This simplified version of the problem has been studied and solved by Ranger [33]. The analogous problem for the sphere was discussed more recently by Pozrikidis [56].

A soft cell migrating over a substrate has peculiar mechanical features, which we now explain. The cell-substrate interface divides the system into two, individuating intracellular and extracellular forces and flows. Intracellular forces originate from the active behaviour of the cell and the cytoskeleton. They are responsible for cell oscillations but do not contribute directly to the cell migration, due to the confining effect of the cell boundary. In our model, only substrate-mediated interactions

are responsible for net translational motion of the cell relative to the substrate, which occurs thanks to the stress transmitted via the substrate. However, both the dissipation associated to the intracellular forces and that associated to the extracellular forces must be included as local contributions. This is at the origin of the biphasic behaviour as a function of the substrate viscosity in our model.

To see this, we consider the four-disks system of Fig.1. We write the force balance for the disks as

$$\mathbf{F}_n^\alpha = \zeta(\dot{\mathbf{x}}_n^\alpha - \mathbf{v}(\mathbf{x}_n^\alpha)) + \boldsymbol{\lambda}_n^\alpha \quad (\text{B1})$$

where the new terms $\boldsymbol{\lambda}_n^\alpha$ are Lagrange multipliers that prevent net motion of the centre of the collection of disks with respect to the cell frame, representing e.g. the interaction with the cell boundary which is not explicitly included in our model. As in the main text, $\zeta = \zeta_s + \zeta_c$ is the total drag coefficient ; $\dot{\mathbf{x}}_n^\alpha$ is the velocity of particle n ; $\mathbf{v}(\mathbf{x}_n^\alpha)$ is the flow at particle (α, n) due to all the remaining force centres.

We identify the non-local, intracellular-mediated, force acting on particle (α, n) : $\mathcal{C}(\mathbf{x}_n^\alpha) := \zeta_c \mathbf{v}(\mathbf{x}_n^\alpha)$. This force is felt by the disk (α, n) at position \mathbf{x}_n^α , due to all the remaining particles and represents a non-local effect mediated by the intracellular environment. Similarly, we identify the non-local, substrate-mediated, force acting on particle (α, n) as $\mathcal{S}(\mathbf{x}_n^\alpha) := \zeta_s \mathbf{v}(\mathbf{x}_n^\alpha)$. The meaning is analogous: $\mathcal{S}(\mathbf{x}_n^\alpha)$ is the force felt by particle (α, n) (at position \mathbf{x}_n^α) due to all the remaining particles representing a non-local effect mediated by the substrate (extracellular environment).

We write Eq.(B1) inserting these definitions of non-local intracellular and extra cellular forces and rearranging terms, $\zeta \dot{\mathbf{x}}_n^\alpha = \mathbf{F}_n^\alpha + \mathcal{C}(\mathbf{x}_n^\alpha) + \mathcal{S}(\mathbf{x}_n^\alpha) - \boldsymbol{\lambda}_n^\alpha$. The Lagrange multipliers $\boldsymbol{\lambda}_n^\alpha$ are determined by requiring : i) no net relative motion between the centre of the system of oscillating units and the cell boundary ; ii) that the oscillatory dynamics of each dipole d_α remains unaffected.

Condition i) is implemented by taking the sum over all the particles in the previous equation. By definition the system is force-free, so the sum of all the active forces driving the particles vanishes, $\sum_{n=1}^2 \sum_{\alpha=A,B} \mathbf{F}_n^\alpha = 0$. Again by definition, $\sum_{n=1}^2 \sum_{\alpha=A,B} \dot{\mathbf{x}}_n^\alpha = 4\dot{\mathbf{c}}$. Condition ii) reads $\sum_{n=1}^2 \sum_{\alpha=A,B} \mathcal{C}(\mathbf{x}_n^\alpha) = \sum_{n=1}^2 \sum_{\alpha=A,B} \boldsymbol{\lambda}_n^\alpha$. Together these result in

$$\dot{\mathbf{c}} = \frac{1}{4} \frac{\zeta_s}{(\zeta_s + \zeta_c)} \sum_{\alpha=A,B} \sum_{n=1,2} \mathbf{v}(\mathbf{x}_n^\alpha) \quad (\text{B2})$$

In addition, condition ii) implies $\boldsymbol{\lambda}_1^\alpha = \boldsymbol{\lambda}_2^\alpha$ for $\alpha = A, B$ so each oscillating unit satisfies

$$\zeta \dot{\mathbf{d}}_\alpha = \mathbf{F}_1^\alpha - \mathbf{F}_2^\alpha + \zeta[\mathbf{v}(\mathbf{x}_1^\alpha) - \mathbf{v}(\mathbf{x}_2^\alpha)]. \quad (\text{B3})$$

Analogous expressions can be obtained for the eight disks system, see [45].

2. Elastic cells on viscous substrates

We return to the case of disks bound to an elastic cell body. The equation describing the dynamics of one isolated disk, centred at position $\mathbf{x}^{(eq)}$, at the interface between elastic cell and viscous substrate is given by $-\zeta_s \dot{\mathbf{x}} - \xi_c[\mathbf{x} - \mathbf{x}^{(eq)}] + \mathbf{f} = 0$. Here ζ_s describes the substrate viscous drag as before and ξ_c the coefficient relating deformation and force applied to the centre of a disk [57] lying at the interface (for a disk of radius a , $\xi_c = \frac{16}{3}a\mu_c$). This expression can be readily generalised to the case of many disks, labeled as before with indices α and n , as $-\zeta_s[\dot{\mathbf{x}}_n^\alpha - \mathbf{v}(\mathbf{x}_n^\alpha)] - \xi_c[\mathbf{x}_n^\alpha - \mathbf{x}_n^{(eq),\alpha} - \mathbf{u}(\mathbf{x}_n^\alpha)] + \mathbf{F}_n^\alpha = 0$. $\mathbf{v}(\mathbf{x}_n^\alpha)$ and $\mathbf{u}(\mathbf{x}_n^\alpha)$ represent the velocity field in the substrate and the deformation field in the cell at the location of disk α, n . From these equations the dynamics of each oscillating units $\alpha = A, B$ is obtained as

$$\dot{\mathbf{d}}_\alpha = \frac{[\mathbf{F}_1^\alpha - \mathbf{F}_2^\alpha]}{\zeta_s} - \frac{\xi_c}{\zeta_s} \mathbf{d}_\alpha + \mathbf{v}(\mathbf{x}_1^\alpha) - \mathbf{v}(\mathbf{x}_2^\alpha) + \frac{\xi_c}{\zeta_s} [\mathbf{u}(\mathbf{x}_1^\alpha) - \mathbf{u}(\mathbf{x}_2^\alpha)] \quad (\text{B4})$$

Since the disks are rigidly connected to the elastic body, the terms $\boldsymbol{\lambda}_n^\alpha$ used above to enforce the average disk locations with respect to the cell boundaries are not needed. The migration speed is obtained by studying the motion of tracers lying in the substrate, below the disks, at $z \rightarrow 0^-$. We need four tracers for the four disks system and eight tracers for the eight disks. The tracers are convected by the flow underneath the disks so the tracer dynamics is described by $-\zeta_s[\dot{\mathbf{x}}_n^\alpha - \mathbf{v}(\mathbf{x}_n^\alpha)] = 0$. Thus the centre of the collection of tracers moves according to

$$\dot{\mathbf{c}} = \frac{1}{4} \sum_{\alpha=A,B} \sum_{n=1}^2 \mathbf{v}(\mathbf{x}_n^\alpha) \quad (\text{B5})$$

where $\mathbf{v}(\mathbf{x}_n^\alpha)$ is given by Eq.(A5). This expression describes the propulsive speed of the cell.

3. Force-dipole and quadrupole

From now on, we restrict ourselves to the one-dimensional force distribution discussed in the main text. Just like in the main text, the disks are centred at positions \mathbf{x}_n^α and subjected to forces F_n^α which satisfy $f^\alpha := F_1^\alpha = -F_2^\alpha$, for $\alpha = A, B$. The coordinates can be written as

$$x_n^A = c - \frac{r}{2} + (-)^{n+1} \frac{L_A}{2}; \quad x_n^B = c + \frac{r}{2} + (-)^{n+1} \frac{L_B}{2} \quad (\text{B6})$$

where $r = c_B - c_A$ is the separation between the centres of the two oscillating units, see Fig.1, and $(-)^n = (-1)^n$. The quantities c and L_α are the crawler's centre and the (time-dependent) length of dipole α . With no loss of generality we pose $L_\alpha = l_\alpha + d_\alpha$ where l_α is a constant and d_α is time-varying as in Eq.(3).

The force-multipoles are defined as moments of the force distribution. To illustrate this we consider Eq.(B6). The moment of order k is $\mathcal{M}^{(k)} := \sum_{\alpha=A,B} \sum_{n=1,2} F_n^\alpha (x_n^\alpha - c)^k$. We pose $\mathcal{D} := \mathcal{M}^{(1)}$, for the dipole, and $\mathcal{Q} := \mathcal{M}^{(2)}$, for the quadrupole, and find that they are given by the matrix relation

$$\begin{pmatrix} \mathcal{D} \\ \mathcal{Q} \end{pmatrix} = \begin{pmatrix} L_A & L_B \\ -rL_A & rL_B \end{pmatrix} \cdot \begin{pmatrix} f_A \\ f_B \end{pmatrix} \quad (\text{B7})$$

showing that the total dipole \mathcal{D} of the system is the sum of the two individual dipoles. In turn, the two forces f_A and f_B can be expressed as functions of dipole and quadrupole moments as

$$\begin{pmatrix} f_A \\ f_B \end{pmatrix} = \frac{1}{2} \begin{pmatrix} \frac{1}{L_A} & -\frac{1}{rL_A} \\ \frac{1}{L_B} & \frac{1}{rL_B} \end{pmatrix} \cdot \begin{pmatrix} \mathcal{D} \\ \mathcal{Q} \end{pmatrix}. \quad (\text{B8})$$

This relation implies that higher moments $\mathcal{M}^{(n)}$, with $n > 2$, can be expressed as combinations of the two moments \mathcal{D} and \mathcal{Q} .

4. Migration speed

To begin with, we note that the flow generated at position x_n^α (the centre coordinate of the generic disk (n, α)) by all the remaining disks can be written as

$$v(x_n^\alpha) = \sum_{m \neq n} H_{n\alpha m\alpha} F_m^\alpha + \sum_{\beta \neq \alpha} \sum_{m=1,2} H_{n\alpha m\beta} F_m^\beta \quad (\text{B9})$$

where we have introduced $H_{n\alpha m\beta} := H(x_n^\alpha - x_m^\beta) \equiv \frac{1}{2\pi(\eta_s + \eta_c)|x_n^\alpha - x_m^\beta|}$ as obtained in Section A 1.

a. Instantaneous migration speed

From the force balance, using Eq.(B2) and the expression in Eq.(B9) we obtain the instantaneous migration speed for the system depicted in Fig.1 as

$$\dot{c} = \frac{\zeta_s}{\zeta} \frac{1}{4} [(H_{1A1B} - H_{1A2B} + H_{2A1B} - H_{2A2B})f_B + (H_{1B1A} - H_{1B2A} + H_{2B1A} - H_{2A2B})f_A]. \quad (\text{B10})$$

b. Approximate expression for instantaneous migration speed

An approximate analytical expression for the migration speed is obtained by performing the analogue of a multipole expansion, valid for $2r \gg |L_A + L_B|$, up to third order in the separation r

$$\dot{c} \approx \frac{\zeta_s}{\zeta} \frac{1}{4} \left\{ 2H'[L_B f_B - L_A f_A] + \frac{1}{12} H''' [(L_B^3 + 3L_A^2 L_B) f_B - (L_A^3 + 3L_A L_B^2) f_A] \right\} \quad (\text{B11})$$

where we defined $H' := \frac{d}{dr} H(r)$ and $H''' := \frac{d^3}{dr^3} H(r)$.

c. Instantaneous migration speed and dipole/quadrupole moments

We now briefly discuss how the migration speed is related to the dipole and quadrupole term of the force-distribution. Inserting the expression of f_A and f_B as functions of \mathcal{D} and \mathcal{Q} obtained from the second relation of Eq.(B8) we obtain

$$\dot{c} \approx \frac{\zeta_{sub}}{2\zeta} \left\{ H' \frac{\mathcal{Q}}{r} + \frac{H'''}{24} [(L_A^2 - L_B^2) \mathcal{D} + 2(L_A^2 + L_B^2) \frac{\mathcal{Q}}{r}] \right\}. \quad (\text{B12})$$

Eq.(B12) shows that, to leading order in the separation r , the sign of the instantaneous migration speed is determined by the quadrupole, consistently with what reported in [26]. Since here the terms f_α and d_α with $\alpha = A, B$ are oscillating quantities with zero mean, the same holds for dipole and quadrupole \mathcal{D}, \mathcal{Q} . As a consequence, also the first term of Eq.(B12) oscillates with zero mean and does not contribute to the net migration speed. A net contribution comes instead from the remaining terms in Eq.(B12) which depend again on dipole or quadrupole but are more involved. Ref. [26] does not report how the average migration speed depends on the dipole or quadrupole so a direct comparison with experiments is not yet available in this case.

d. Approximated expression for the average migration speed

To obtain the average migration speed we insert the parametrisation of Eq.(3) in Eq.(B11) and take the average over the period $T := \frac{2\pi}{\omega}$. In doing so, for example, we find that the term $L_A f_A - L_B f_B$ contains a combinations of $e^{i\omega t}$ and $e^{-i\omega t}$ and therefore vanishes when we average over the period T as discussed above. For the same reason, the term $L_A^3 f_A - L_B^3 f_B$ does not contribute. Instead, the remaining term gives a finite contribution to the average as $L_A L_B (L_A f_B - L_B f_A) \sim [2l^2 + d_A d_B] (d_A f_B - d_B f_A)$ where \sim neglects terms that average to zero. In particular, we find $d_A f_B - d_B f_A \sim -\frac{1}{2} \zeta \omega R_A R_B \sin \psi$ where $\psi := \phi_B - \phi_A$. Similarly $d_A d_B [d_A f_B - d_B f_A] \sim -\frac{\zeta \omega}{8} R_A^2 R_B^2 \sin 2\psi$. Hence, to leading order in the multipole expansion the average migration speed in a period T is the expression reported in the main text, Eq.(4), where

$$\Xi := \frac{3}{32\pi} [4 + \frac{R_A R_B}{l^2} \cos \psi] = \frac{3}{32\pi} [4 + \frac{4g_A g_B}{l^2 \omega^2 \zeta^2} \cos \psi]. \quad (\text{B13})$$

The last equality holds by virtue of the relation among deformation and force $g_\alpha = (\zeta R_\alpha \omega)/2$ valid at lowest order in a/L_α .

To produce a plot we arbitrarily choose a phase shift $\psi = \pi/2$ between the oscillators. For a disk $\zeta = [16a(\eta_s + \eta_c)]/3$. Moreover, we pose $R_A = R_B = R$ and $g_A = g_B = g$. So, in the case where oscillations are driven by providing fixed oscillation amplitude R we obtain $v_c = \frac{\eta_s}{(\eta_s + \eta_c)r^4} \frac{1}{\pi} a \omega l^2 R^2$. Instead, if oscillations are driven by providing fixed force amplitude g we get $v_c = \frac{\eta_s}{(\eta_s + \eta_c)^3 r^4} \frac{1}{a \omega} \frac{9}{64\pi} l^2 g^2$. To distinguish between these two cases we further pose $\Xi_g := \frac{1}{\eta_c^2} \frac{1}{a \omega} \frac{9}{64\pi} l^2 g^2$ and $\Xi_R := \frac{1}{\pi} a \omega l^2 R^2$ and measure the migration speed respectively in units of $\frac{\Xi_R}{r^4}$ or in units of $\frac{\Xi_g}{r^4}$, keeping η_c constant and varying η_s see Fig.(2)(a). A different choice for the phase shift, $\psi \neq 0, \pi$, will introduce corrections associated to the term $\cos \psi$ in Ξ . As the amplitudes of oscillation must satisfy $R < l$, these corrections do not affect the qualitative trend of the migration speed although they can shift the value of substrate viscosity at which the migration is optimal, as well as the maximum speed.

e. Approximated expression for the average migration speed for elastic cells on viscous substrates

In this case Eq.(B5) depends on $\mathbf{v}(\mathbf{x})$ given by Eq.(A5) and contains the sum of two terms. The first term resembles what was found for the viscous cell lying on the viscous substrate. The second term describes the contribution of the elastic interactions. It is important to note that such a term contains an exact time-derivative, of periodic functions of period $T = \frac{2\pi}{\omega}$. Thanks to that, the average over one period gives $\int_0^T dt \partial_t [\mathbf{G}^{(e)} \cdot \mathbf{F}] = \mathbf{G}^{(e)} \cdot \mathbf{F}|_{t=T} - \mathbf{G}^{(e)} \cdot \mathbf{F}|_{t=0} \equiv 0$. Thus for calculating the average speed we can approximate $\mathbf{v}(\mathbf{x}) \sim \mathbf{H}^{(e)} \cdot \mathbf{F}$ in Eq.(A5). The multipole expansion for the elastic cell is identical to the one obtained for the viscous cell, Eq.(B11) (and related Eq.(B12)). The difference is that for the elastic cell forces f_α and deformations d_α satisfy a relation which follows from Eq.(B4). Neglecting, as before, the effect of the interactions at this level, Eq.(B4) yields a local relation between forces and displacements of the oscillators $\dot{d}_\alpha = -\frac{1}{\mathcal{T}} d_\alpha + \frac{2}{\zeta_s} f_\alpha$ where $\mathcal{T} := \frac{\eta_s}{\mu_c}$ is the timescale obtained combining the elastic modulus of the cell and the viscosity of the substrate. Note that μ_c/ω has the dimension of a viscosity, so $\omega \mathcal{T} = \frac{\omega \eta_s}{\mu_c}$ is equivalent to a viscosity ratio. We obtain different force-deformation relations depending on the chosen prescription. In particular we note the parametrisation given in Eq.(3) needs to be modified to include the additional timescale \mathcal{T} , see below.

Assigning forces. If we assign forces as $f_\alpha = -g_\alpha \sin(\omega t + \phi_\alpha)$ then displacements are obtained solving the differential equation for d_α , whose solution at the steady state is $d_\alpha(t) \sim -\frac{2}{\zeta_s} g_\alpha \frac{\mathcal{T}}{1 + \omega^2 \mathcal{T}^2} [\sin(\omega t + \phi_\alpha) - \omega \mathcal{T} \cos(\omega t + \phi_\alpha)]$. As for a viscous cell, the dipole term does not contribute to the mean speed while the quadrupole does. Posing again $g_\alpha = g$ and $f_\alpha = f$ for

$\alpha = A, B$ the result is

$$v_c(\psi) = \frac{3\eta_s g^2 \mathcal{T}^2 l^2 \omega [(1 + \omega^2 \mathcal{T}^2) + (\frac{g \mathcal{T}}{\zeta_s})^2 \cos \psi] \sin \psi}{\eta_s^2 + \frac{\mu_c^2}{\omega^2}} \frac{4\pi \zeta_s r^4 (1 + \omega^2 \mathcal{T}^2)^2}{(B14)}$$

Note that the term $(\frac{g \mathcal{T}}{\zeta_s})$ has the dimension of length, and describes the oscillation amplitude d_α . Therefore it must satisfy $(\frac{g \mathcal{T}}{\zeta_s}) < l$. Studying the behaviour as a function of η_s we recover the non-monotonic trend found for the case of fluid cell, peaked around $\eta_s \sim \frac{\mu_c}{\omega}$. It is interesting to note that this migration speed is also a non-monotonic function of ω , peaked around $\omega \sim \frac{2}{\mathcal{T}}$ (weakly sensitive to the values of ψ and to the ratio $(\frac{g \mathcal{T}}{\zeta_s l})$). This result suggests a cell may adapt its oscillation frequency to the environment in order to optimise its speed. To produce a plot as a function of the frequency, in this case we consider the expression of v_c given by Eq.(B14) for the value $\psi = \pi/2$ as before, obtaining $v_c = \frac{3}{4\pi} \frac{l^2 g}{\eta_s r^4} (\frac{g}{\zeta_s}) \frac{\omega^3 \mathcal{T}^3}{(1 + \omega^2 \mathcal{T}^2)^2}$. Fig.2(b) of the main text shows v_c in unit of the velocity $\frac{3}{4\pi} \frac{l^2 g}{\eta_s r^4} (\frac{g}{\zeta_s})$ measuring ω in units of \mathcal{T}^{-1} .

The physical reason beyond the existence of an optimal frequency in the case of prescribed forces can be understood using a simple argument [58]. The propulsion (and pumping of fluid) are proportional to terms that contain product of forces, f_α , and deformations, d_α , of the oscillators. Imposing the force, in presence of viscoelasticity, the deformations take place on typical timescale \mathcal{T} . Then: (i) for sufficiently high frequencies, $T \ll \mathcal{T}$, the oscillator cannot reach the maximum amplitude of oscillations. In this regime the allowed amplitude of deformation increases at increasing T (i.e. at decreasing ω); (ii) on the contrary for sufficiently small frequencies, $T \gg \mathcal{T}$, the oscillator can reach the maximum amplitude available. So in this regime the amplitude of deformation does not vary at increasing T . To calculate the average speed we must divide d_α by T . The resulting function in regime (i) can increase at increasing T while in regime (ii) only decreases at increasing T (behaving as $\sim \text{constant}/T$). The optimal frequency lies at the crossover between these two regions. The situation is different when deformations are prescribed functions.

Assigning deformations. If we assign deformations as $d_\alpha(t) = R \cos(\omega t + \phi_\alpha)$ The forces are also prescribed functions of time, directly related to the deformations via $f_\alpha = \frac{\zeta_s}{2} [\dot{d}_\alpha + \frac{d_\alpha}{\mathcal{T}}]$ which yields $f_\alpha(t) = R \frac{\zeta_s}{2\mathcal{T}} [-\omega \mathcal{T} \sin(\omega t + \phi_\alpha) + \cos(\omega t + \phi_\alpha)]$. Also here only the quadrupole contributes to the average as

$$v_c(\psi) = \frac{3}{16\pi} \frac{\eta_s l^2 \omega \mathcal{T}}{\eta_s^2 + \frac{\mu_c^2}{\omega^2}} (\frac{R^2 \zeta_s}{r^4 \mathcal{T}}) [1 + \frac{R^2}{4l^2} \cos \psi] \sin \psi. (B15)$$

Interestingly, also this expression has a maximum as a function of the substrate viscosity but only monotonic trend as a function of ω . Fig.2(b) of the main text shows

the velocity as a function of the frequency for fixed deformation. In this case we consider the expression of v_c

given by Eq.(B15) for the value $\psi = \pi/2$ as before, obtaining $v_c = \frac{1}{\pi} \frac{\omega^3 \mathcal{T}^3}{1 + \omega^2 \mathcal{T}^2} \frac{R^2 l^2}{r^4} \frac{a}{\mathcal{T}}$. We plot v_c in units of the velocity $\frac{1}{\pi} \frac{R^2 l^2}{r^4} \frac{a}{\mathcal{T}}$ measuring ω in units of \mathcal{T}^{-1} .

-
- [1] D. Bray, *Cell Movements: from Molecules to Motility* (Garland Science (New York), 1992).
 - [2] E. Lauga and T. R. Powers, Rep. Prog. Phys. **72**, 096601 (2009).
 - [3] N. P. Barry and M. S. Bretscher, PNAS **107**, 11376 (2010).
 - [4] J. D. Howe, N. P. Barry, and M. S. Bretscher, PLOS One **8**, e74382 (2013).
 - [5] M. Gardel, B. Sabass, L. Ji, G. Danuser, U. Schwarz, and C. Waterman, J Cell Biol **183**, 999 (2008).
 - [6] K. M. Stroka and H. Aranda-Espinoza, Cell Motility and the Cytoskeleton **66**, 328 (2009).
 - [7] A. Pathak and K. Sanjay, PNAS **109**, 10334 (2012).
 - [8] A. P. Kourouklis, R. V. Lerum, and H. Bermudez, Bio-materials **35**, 4827 (2014).
 - [9] C. Muller, A. Muller, and T. Pompe, Soft Matter **9**, 6207 (2013).
 - [10] A. Farutin *et al.*, Phys. Rev. Lett. **111**, 228102 (2013).
 - [11] K. F. Swaney, C. H. Huang, and P. N. Devreotes, Annu. Rev. Biophys **39**, 265 (2010).
 - [12] C. M. Lo, H. B. Wang, M. Dembo, and Y. L. Wang, Biophys. J. **79**, 144 (2000).
 - [13] J. van der Gucht and C. Sykes, Cold Spring Harb Perspect Biol **1**, a001909 (2009).
 - [14] K. Sekimoto *et al.*, EPJE **13**, 247 (2004).
 - [15] K. Kruse *et al.*, Physical Biology **3**, 130 (2006).
 - [16] F. Ziebert, S. Swaminathan, and I. S. Aranson, J. R. Soc. Interface **9**, 1084 (2011).
 - [17] E. Tjhung, D. Marenduzzo, and M. E. Cates, PNAS **109**, 12381 (2012).
 - [18] M. M. Kozolov and A. Mogilner, Biophysical Journal **93**, 3811 (2007).
 - [19] J. F. Joanny and S. Ramaswamy, J. Fluid Mech. **705**, 46 (2012).
 - [20] T. Killich *et al.*, J. Cell Sci. **106**, 1005 (1993).
 - [21] L. Ji, J. Lim, and G. Danuser, Nat. Cell Biol. **10**, 1393 (2008).
 - [22] B. R. Graziano and O. D. Weiner, Curr. Opin. in Cell Biol. **30**, 60 (2014).
 - [23] S. Ghassemi *et al.*, PNAS **109**, 5328 (2012).
 - [24] B. Ladoux and A. Nicolas, Rep. Prog. Phys. **75**, 116601 (2012).
 - [25] U. S. Schwarz and S. A. Safran, Rev. Mod. Phys. **85**, 1327 (2013).
 - [26] H. Tanimoto and M. Sano, Biophys. J. **106**, 16 (2014).
 - [27] C. G. Galbraith and M. P. Sheetz, Proc Natl Acad Sci USA **94**, 9114 (1997).
 - [28] G. Giannone, B. J. Dubin-Thaler, H.-G. Döbereiner, N. Kieffer, A. R. Bresnick, and M. P. Sheetz, Cell **116**, 431 (2004).
 - [29] T. Lammermann *et al.*, Nature **453**, 51 (2008).
 - [30] E. Lifshitz and L. Landau, *Course of Theoretical Physics*, volume VI: *Fluid Mechanics* (Butterworth-Heinemann, 1987).
 - [31] D. K. Lubensky and R. E. Goldstein, Phys. Fluids **8**, 843 (1996).
 - [32] P. Lenz, J.-F. Joanny, F. Jülicher, and J. Prost, Eur. Phys. J. E **13**, 379 (2004).
 - [33] K. B. Ranger, Int. J. of Multiphase Flow **4**, 263 (1978).
 - [34] R. Golestanian and A. Ajdari, Phys Rev E **77**, 036308 (2008).
 - [35] E. Lauga and D. Bartolo, Phys. Rev. E **78**, 030901 (2008).
 - [36] G. P. Alexander and J. M. Yeomans, Eurohys. Lett. **83**, 34006 (2008).
 - [37] E. M. Purcell, American journal of Physics **45**, 3 (1977).
 - [38] B. Fabry *et al.*, Phys. Rev. Lett. **87**, 148102 (2001).
 - [39] A. Pikovsky, M. Rosenblum, and J. Kurths, *Synchronization - A Universal Concept in Nonlinear Science* (Cambridge University Press, 2002).
 - [40] M. Leoni and T. B. Liverpool, Phys. Rev. E **85**, 040901(R) (2012).
 - [41] J. Guckenheimer and P. Holmes, *Nonlinear Oscillations, Dynamical Systems, and Bifurcations of Vector Fields* (Springer-Verlag, 2002).
 - [42] F. Jülicher and J. Prost, Phys. Rev. Lett. **78**, 4510 (1997).
 - [43] T. Guerin, J. Prost, and J. F. Joanny, Eur. Phys. J. E **34**, 60 (2011).
 - [44] M. P. Neilson *et al.*, Plos Biology **9**, e1000618 (2011).
 - [45] See Supplemental Material at [URL will be inserted by publisher] for details of the calculations..
 - [46] R. E. Goldstein, M. Polin, and I. Tuval, Phys. Rev. Lett. **103**, 168103 (2009).
 - [47] B. M. Friedrich and F. Jülicher, Phys. Rev. Lett. **109**, 138102 (2012).
 - [48] R. R. Bennett and R. Golestanian, Phys. Rev. Lett. **110**, 148102 (2013).
 - [49] H. C. Berg and D. A. Brown, Nature **239**, 500 (1972).
 - [50] P. Hänggi, P. Talkner, and M. Borkovec, Rev. Mod. Phys. **62**, 251 (1990).
 - [51] G. Amselem, M. Theves, A. Bae, E. Bodenschatz, and C. Beta, PloSOne **7**, e37213 (2012).
 - [52] M. Abramowitz and I. A. Stegun, *Handbook of Mathematical Functions* (Dover, 1964).
 - [53] A. J. Levine, T. B. Liverpool, and F. C. MacKintosh, Phys. Rev. Lett. **93**, 038102 (2004).
 - [54] M. Leoni and T. Liverpool, EPL **92**, 64004 (2010).
 - [55] P. G. Saffman and M. Delbruck, PNAS **72**, 3111 (1975).
 - [56] C. Pozrikidis, J. Fluid Mech. **575**, 333 (2007).
 - [57] D. C. Lin, N. A. Langranaa, and B. Yurke, J. Appl. Phys. **97**, 043510 (2005).
 - [58] M. Leoni, B. Bassetti, J. Kotar, P. Cicuta, and M. Cosentino Lagomarsino, Phys. Rev. E **81**, 036304 (2010).